

Plastic mechanism analysis of vehicle roof frames consisting of spot-welded steel hat sections

M.R. Bambach*

Transport and Road Safety (TARS), Faculty of Science, Old Main Building, University of New South Wales, Sydney, NSW 2052, Australia

(Received September 25, 2013, Revised May 5, 2014, Accepted May 27, 2014)

Abstract. Plastic mechanism analysis of structures subjected to large deformation has long been used in order to determine collapse mechanisms of steel structures, and the energy absorbed in plastic deformation during such collapses. In this paper the technique is applied to vehicle roof structures that undergo large plastic deformation as a result of rollover crashes. The components of such roof structures are typically steel spot-welded hat-type sections. Ten different deformation mechanisms are defined from investigations of real-world rollover crashes, and an analytical technique to determine the plastic collapse load and energy absorption of such mechanisms is determined. The procedure is presented in a generic manner, such that it may be applied to any vehicle structure undergoing a rollover induced collapse. The procedure is applied to an exemplar vehicle, in order to demonstrate its application in determining the energy absorbed in the deformation of the identified collapse mechanisms. The procedure will be useful to forensic crash reconstructionists, in order to accurately determine the initial travel velocity of a vehicle that has undergone a rollover and for which the post-crash vehicle deformation is known. It may also be used to perform analytical studies of the collapse resistance of vehicle roof structures for optimisation purposes, which is also demonstrated with an analysis of the effect of varying the geometric and material properties of the roof structure components of the exemplar vehicle.

Keywords: plastic mechanism analysis, energy absorption, roof collapse, bending collapse, vehicle rollover

1. Introduction

Vehicle rollover crashes are the cause of many fatalities and severe head, neck and spine trauma around the world. Since 2000 in the United States alone, up to 10,000 people every year have been killed in vehicle rollover accidents (NHTSA 2013), and in Australia one in every three to four vehicle fatalities involves a rollover of the vehicle (Young *et al.* 2007). An important part of understanding vehicle crashes and reconstructing crashes for forensic purposes is determining how the initial kinetic energy of the vehicle was dissipated during the crash. For example in frontal crashes, skid distances and frontal crush deformations are used to estimate the travel velocity of the vehicle (Sharma *et al.* 2007). Such calculations are important for legal reasons (i.e., to establish

*Corresponding author, Ph.D., E-mail: m.bambach@unsw.edu.au

liability for the crash if a speed infraction occurred), and are especially important for crash research purposes where the change in velocity (delta-V) that occurred during the crash may be related to many factors, such as injury risk. For example the United States National Automotive Sampling System (NASS) Crashworthiness Data System (CDS), the principle in-depth crash reconstruction database in the US, uses damage analysis and/or trajectory analysis to establish the delta-V of the crash. In this database 99% of calculated delta-V values use damage analysis for the calculation, of which 58% use damage analysis only and the remaining use both damage and trajectory analyses (Sharma *et al.* 2007). While such techniques are well established and widely used for frontal crashes, relatively little is understood for the rollover crash mode where vehicle deformation and energy dissipation occurs in the roof structure components, and no analytical techniques are currently available to estimate the magnitude of this energy. Consequently, current rollover crash reconstruction techniques do not consider this component of energy dissipation and the initial travel velocity of the vehicle may only be crudely estimated from the roll distance using the so-called Kildare Curves. While vehicle damage is documented in detail in the NASS CDS, delta-V estimates for vehicle rollover crashes are not calculated due to the unreliability of this method (NHTSA 2012). The aim of the present paper is to establish analytical techniques to estimate the rollover energy dissipated in roof deformation, and thereby improve the accuracy of forensic crash reconstruction techniques for vehicle rollover crashes. Additionally, a better understanding of the energy dissipation and how the design of the roof structure components influence it may lead to improvements in roof structure design for reducing occupant injuries, since some injury modes have been shown to be related to the magnitude of roof deformation (Bambach *et al.* 2013).

The problem has been addressed in three stages: in the first stage an assessment of real-world vehicle roof member profiles was performed to determine representative pillar and roof rail dimensions for vehicles involved in rollover crashes (Tan *et al.* 2008); in the second stage experiments of spot-welded thin-walled steel hat sections with representative dimensions were performed to assess the effect of section geometry and perforations on the large deformation bending strength, and theoretical models were developed (Bambach *et al.* 2009); the results of the third stage are reported in the present paper, where the theoretical models are combined with plastic mechanism theories for frames, and applied to real-world rollover crash mechanisms and an exemplar vehicle. Plastic mechanism analysis of structures subjected to large deformation has long been used in order to determine collapse mechanisms of steel structures, and the energy absorbed in plastic deformation during such collapses (Kecman 1983, Elchalakani *et al.* 2002, Elchalakani 2007, Setiyono 2007, Ye *et al.* 2007, Kotelko 2008, Ungureanu *et al.* 2010, Elchalakani and Fernando 2012, Maduliat *et al.* 2012). Ten typical plastic collapse mechanisms of vehicle roof frames resulting from rollover crashes were identified from a real-world crash database. The theoretical method used to determine the energy absorbed under large deformation bending of a particular element of the roof structure was based upon the previous experimental and analytical investigation of spot-welded steel hat sections (Bambach *et al.* 2009). The procedure may be applied to particular roof structures with known crash deformation, and the energy dissipated by the roof structure during the rollover may be estimated. Various material and geometric variables may also be modified to perform optimisation studies, to investigate their effect on the collapse load and energy absorbing potential of the roof structure in a vehicle rollover crash. The application of the procedures are demonstrated with a late model exemplar vehicle.

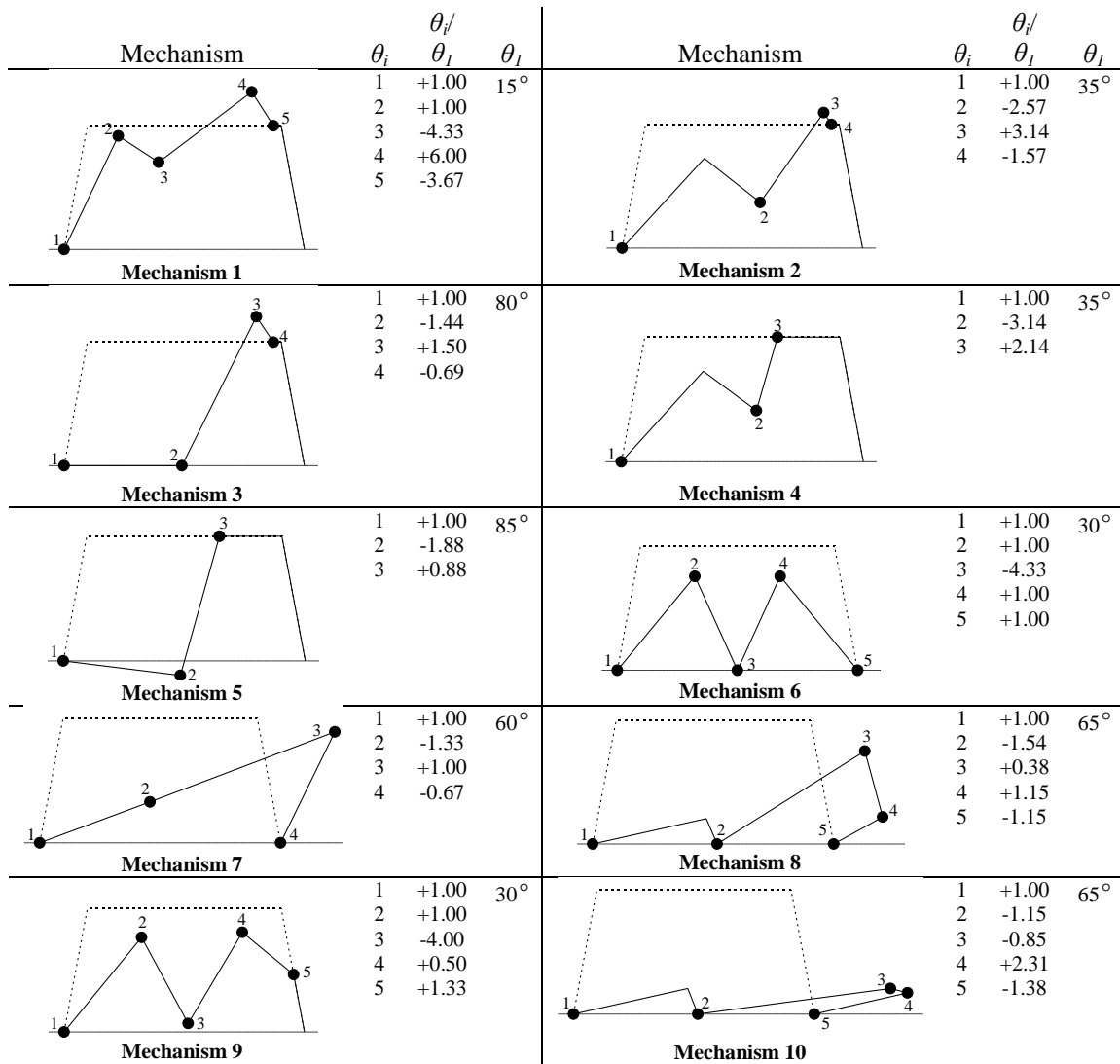


Fig. 1 Idealised rollover-induced vehicle roof frame plastic collapse mechanisms, scaled to the geometry of the exemplar vehicle (θ_i is the rotation of hinge i and θ_j is the rotation of hinge j)

2. Roof structure failure mechanisms resulting from vehicle rollover crashes

The United States National Highway Traffic Safety Administration (NHTSA) maintains the Crashworthiness Data System (CDS), in which around 5,000 road crashes are investigated in detail per year (NHTSA 2012). This database was searched for fatal single-vehicle rollover crashes that occurred between 2004 and 2009, and photographs of the vehicles were extracted. From these photographs, ten typical rollover induced roof collapse mechanisms were identified and are shown in Fig. 1. The general shapes of the mechanisms were determined from the photographs, and the actual geometry has been adapted to that of the exemplar vehicle (discussed in a later section).

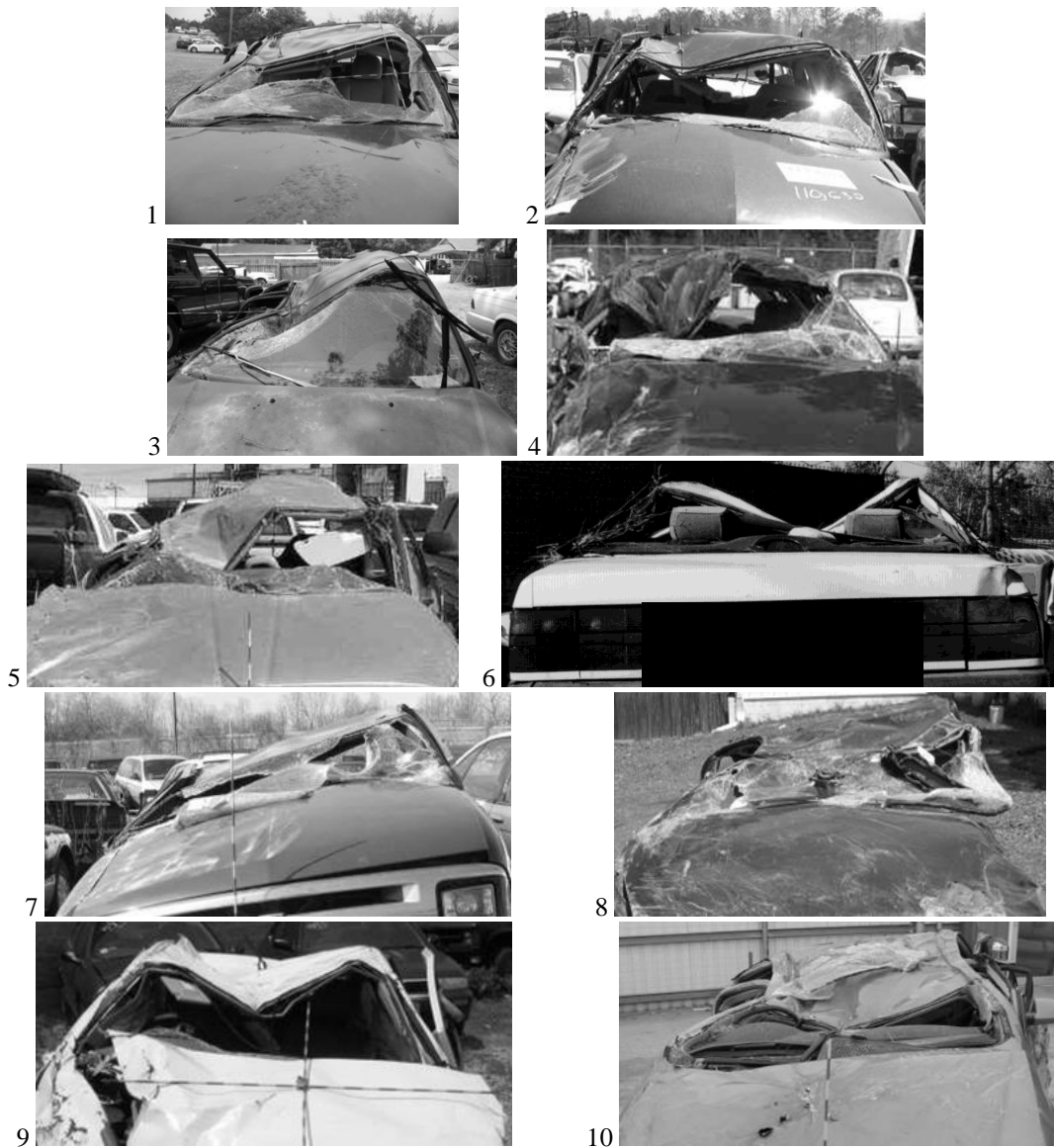


Fig. 2 Post-crash photographs of real-world single vehicle rollover crashes extracted from NHTSA (2012). The photographs from 1 to 10 correspond to the idealised mechanisms from 1 to 10 in Fig. 1

Typical to plastic mechanism analysis, the plastic deformation of the frame is assumed to occur as a result of rotations in a discrete number of plastic hinges, with the remaining portions of the structure remaining straight and inextensible. The energy is thus dissipated in the plastic hinges, and the rotation of each plastic hinge is required and is shown in Fig. 1. Where a hinge is shown at the junction of a pillar and roof rail in Fig. 1, it is assumed that the hinge forms in the roof rail due to the fact that it is much weaker than the pillar (discussed in a later section). Typical to plastic mechanism analysis, the mechanisms are determined from observed mechanisms and some rationalisation must occur in order to simplify the real mechanisms to those shown in Fig. 1.

Examples of real mechanisms that approximately correspond to the idealised mechanisms are presented in Fig. 2.

In Fig. 1, the deformation of the front roof frame is shown, that is the frame consisting of the A-pillars and the front roof rail. Moving towards the rear of the vehicle, most vehicles will also contain B-, C- and sometimes D-pillars, creating additional structural frames when linked with roof rails. In the rollover crashes extracted from the CDS, in many cases the crashes were so severe that all roof frames were deformed in much the same manner as the front roof frame (eg photographs 1, 3, 5, 6, 7, 8 and 10 in Fig. 2). However, in some cases, the front roof frame was the most heavily deformed, with less deformation occurring in the frames moving towards the rear of the vehicle (e.g., photographs 2, 4 and 9 in Fig. 2). If all the structural frames in the roof are assumed to deform by the same amount, then the solid line in Fig. 1 indicates the deformation of all roof frames and the dotted line indicates the original roof frame geometry.

3. Roof structure component large deformation behaviour

Each mechanism in Fig. 1 consists of plastic hinges that form in particular pillars and roof rails, and which are subjected to large rotation pure bending. An analytical procedure previously developed was used (Bambach *et al.* 2009), in which an experimental investigation of thin steel spot-welded hat sections subjected to large deformation pure bending was performed on 24 specimens, with seven different slenderness ratios and four different levels of perforation. The slenderness ratio is the non-dimensionalised width to thickness ratio of the element of the profile in the compression face of the bending, and given by Eq. (1). In Eq. (1) a and t are the flat width and thickness of the element, and f_y is the material yield stress. The dimensions of the tested specimens were determined from an investigation of pillars in a random selection of vehicles (Tan *et al.* 2008). The vehicle profile material thickness was generally in the range 0.8 mm - 1.2 mm, and width to thickness ratios were generally in the range 25 - 100, though could be up to 200. It was also noted in the investigation that many profiles had large perforations, which typically varied between 10% and 60% of the element width (see Fig. 1 in Bambach *et al.* (2009), for example). Since it is well known that element slenderness and perforations affect the strength and energy dissipation of steel sections, a range of width to thickness ratios between 20 and 100 (while maintaining a material thickness of 1mm), and perforations between 0% and 60%, were tested in the experimental investigation in Bambach *et al.* (2009). These experimental results were used to develop a rational design approach to determine the large bending deformation behaviour of thin-walled spot-welded steel sections, and since the slenderness and perforations generally cover the range of those typical to vehicle structure profiles, the procedure is nominally valid to be applied to any vehicle profile. The analytical procedure was shown to compare well and slightly conservatively with the 24 experimental results, with a mean test/predicted ratio and coefficient of variation of 1.16 and 0.15 (Bambach *et al.* 2009).

$$\lambda = \frac{a}{t} \sqrt{\frac{f_y}{250}} \quad (1)$$

The analytical procedure developed in Bambach *et al.* (2009) is summarised in Fig. 3. There are three possible stages in the large deformation bending of thin-walled steel sections; the linear elastic stage, the in-plane plastic stage and the plastic collapse mechanism stage. All steel sections will undergo an initial linear elastic stage, the slope of which is the elastic bending stiffness EI ,

Moment capacity		Rotation capacity/ θ_y
$\lambda \leq \lambda_p$	$M_u = Sf_y$	$R = \left(\frac{\lambda_p}{\lambda}\right)5$
$\lambda_p < \lambda \leq \lambda_y$	$M_u = f_y \left[Z + \left(\frac{\lambda_y - \lambda}{\lambda_y - \lambda_p} \right) (S - Z) \right]$	$R = 1 + \left(\frac{\lambda_y - \lambda}{\lambda_y - \lambda_p} \right) 4$
$\lambda > \lambda_y$	$M_u = f_y \left(\frac{\lambda_y}{\lambda} \right) Z$	$R = 1$
Limits:	(λ_y, λ_p) are (45, 30) and (15, 8) for unperforated and perforated compression elements respectively	(λ_y, λ_p) are (45, 30) for unperforated compression elements, and for perforated compression elements; $R_{perf} = 0.2 \frac{a}{a_{perf}} R \leq R$
$\theta_y = K_y L$ $K_y = \frac{Zf_y}{EI}$		$\lambda = \frac{a}{t} \sqrt{\frac{f_y}{250}}$
Moment-rotation relationship		Energy absorbed to θ_f
Elastic	θ_y, M_u	$W_E = \frac{1}{2} M_u \theta_y$
In-plane plastic	$R\theta_y, M_u$	$W_{IPP} = (R-1)M_u \theta_y$
Collapse	$M = \frac{35am_p}{\sqrt{\theta}}$	$W_C = 70am_p \left(\sqrt{\theta_f + \theta_{max}} - R\theta_y - \sqrt{\theta_{max}} \right)$
$\theta_{max} = \left(\frac{35am_p}{M_u} \right)^2$		$m_p = \frac{f_y t^2}{4}$

Fig. 3 Theoretical procedure for the moment-rotation behaviour and energy dissipation of steel spot-welded hat sections with perforations, subjected to large deformation pure bending (Bambach *et al.* 2009)

where E is the material Young's modulus and I is the second moment of area. For sections that contain elements with large slenderness values (slender sections), the section will not reach the yield moment before it begins its collapse stage, and will thus not develop in-plane plasticity. For sections that contain elements with small slenderness values (compact sections), the section will reach the fully plastic moment, and will maintain an in-plane plastic stage where the plastic moment is maintained for large rotations, after which the collapse stage occurs. This is typically referred to as the ductility of the section, and compact sections will display significant ductility, whereas slender sections will display very little ductility. For intermediate sections (non-compact sections), intermediate behaviour occurs where the section may reach the fully plastic moment but may develop a limited in-plane plastic stage before the collapse stage (Elchalakani *et al.* 2002).

The plastic collapse stage of thin-walled steel sections is the stage where the section develops plastic folding of the walls (Ungureanu *et al.* 2010), which involves the development of a spatial plastic mechanism containing plastic hinge lines as shown in Fig. 4 for the spot-welded hat sections with perforations in Bambach *et al.* (2009). The development of the three stages of large

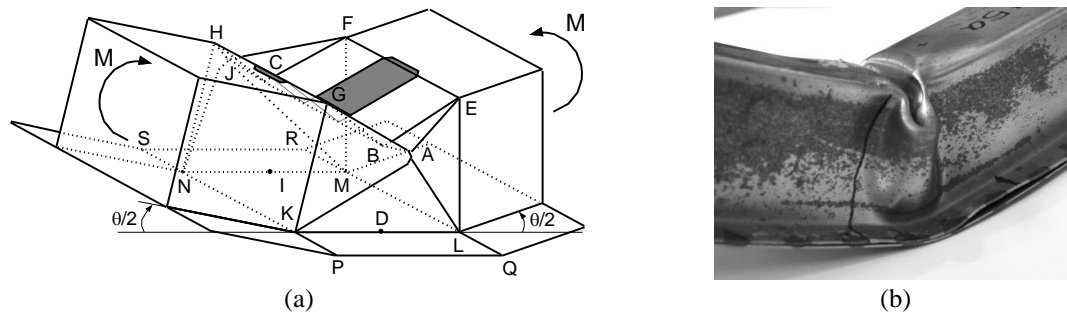


Fig. 4 Plastic collapse mechanism of steel spot-welded hat sections with perforations (Kecman 1983, Bambach *et al.* 2009); a) theoretical and b) observed

deformation behaviour of a thin-walled steel section thus depends on the slenderness values of the elements, and the slenderness limits for the categories of slender, non-compact and compact are given in Fig. 3 (AS 4100 1998). The same limits are used to determine the moment capacity of the section. In non-dimensionalised terms, compact sections will dissipate significantly more energy than slender sections due to the development of in-plane plasticity.

In Fig. 3 the moment capacity equations are those given by the relevant steel specification (Australian in the present case (AS 4100 1998)), and the rotation capacities were defined in Bambach *et al.* (2009). Explicit equations for the plastic collapse behaviour were developed in Bambach *et al.* (2009) for the spatial plastic mechanism shown in Fig. 4, however due to the complexity of these equations an empirical simplification was developed and presented in Fig. 3. Fig. 3 may thus be used to determine the full large deformation moment-rotation curve for any vehicle profile, and this curve may be integrated to determine the energy dissipated under large deformation, the equations for which are also shown in Fig. 3. In the application of Fig. 3 the slenderness ratio (λ) is calculated for the element in compression, and the value of a for the collapse curve is taken as an average of the profile width and depth if the values are similar, or the smaller of the two if they are dissimilar.

4. Calculation of a vehicle roof collapse load and the energy dissipated

The procedure to calculate the collapse load and energy dissipated under large deformation collapse by a vehicle roof structure as a result of a rollover event follows from Figs. 1 and 3. The first step is to determine the appropriate collapse mechanism from Fig. 1. If the analyst wishes to analyse a real-world rollover event, a mechanism should be chosen from Fig. 1 that best represents the observed mechanism. The angles of each of the hinges in the mechanisms in Fig. 1 are presented as a function of the residual (post-crash) pillar angle of the first hinge (θ_1), and the approximate value from the photographs extracted from NHTSA (2012) are shown. The analyst should use the measured value of θ_1 , and may also develop a different mechanism in the event that none of those shown in Fig. 1 are similar to that observed.

Having selected a mechanism and a final mechanism angle, the analyst has thus prescribed a number of plastic hinges in different profiles that undergo plastic rotation of some magnitude. For each profile the corresponding moment-rotation curve may be developed from Fig. 3, up to the prescribed rotation. The geometric and material properties of the profiles are required for this step.

The energy dissipated by each profile is the area under the moment-rotation curve (or determined directly using the equations in Fig. 3), and the energy dissipated by the roof frame is the sum of all the energies of each plastic hinge in each profile.

The collapse load of the frame is determined by equating the internal work to the external work. The internal work is the sum of the work done in each hinge, which is the product of the hinge capacity and the hinge rotation. The external work is determined by assuming the mechanism results from a sideways force applied at the top-left corner of the frame, acting over a displacement defined by the mechanism geometry.

The procedure may also be used to perform optimisation studies of a vehicle roof structure subjected to a typical rollover event, rather than analysing an actual rollover event. In such cases any or all of the mechanisms shown in Fig. 1 may be analysed. The procedure may be used to investigate the effects of various geometric and material parameters of the profiles on the collapse load and energy dissipating potential of a vehicle roof frame under a rollover event, and an example of such follows in the next section. In the same manner, the procedure could also be used to investigate the effect of different strengthening techniques.

5. Application to an exemplar vehicle subjected to a rollover event

In this section a case study is presented of a late model GM Holden sedan subjected to a generic rollover event. The exemplar vehicle was manufactured and sold in the United States from 1998 to 2001, and Australia from 2000 to 2002. It was also sold in the Middle East, Brazil, South Africa, Malaysia, Singapore and Thailand. The roof frame of the exemplar vehicle consists of A-, B-, C- and D-pillars, however the C- and D-pillars connect to a single roof rail. That is, the roof structure consists of three frames that traverse the vehicle from side to side.

5.1 Profile geometry

The profiles of the A-, B-, C- and D- pillars, and the roof rails, were determined from carefully measured sections cut from the vehicle. The full dimensions of the profiles are documented in Tan *et al.* (2008). The quite complicated profiles were rationalised in order to simplify the analysis, and were then entered into cross-section analysis software (Papangelis and Hancock 1995) to determine the geometric properties I (second moment of area), Z (elastic bending modulus) and S (plastic bending modulus). The profile images and values determined from the analysis are presented in Fig. 5. The material was assumed to be mild steel with yield stress 250 MPa. All profiles had a measured steel sheet thickness of 0.9 mm. The lips had thicknesses of 1.8mm or 2.7 mm depending on how many sheets were spot-welded at the lip. The geometric properties are relative to the axis of bending, therefore care was taken in order to orient the profiles in the correct manner according to their position in the vehicle and direction of bending under roof structure collapse. The profiles are thus orientated accurately in Fig. 5, and the inside of the vehicle and the positive moment direction are indicated. For non-symmetric sections the direction of bending is also important, as it determines which element is in compression and thus the section slenderness. The positive moment direction in Fig. 5 is drawn such that it corresponds with the signs of the angles in the mechanisms in Fig. 1. The section slenderness values for positive bending are listed in Fig. 5, where it is clear that the profiles in the exemplar vehicle are generally quite slender. The pillar slenderness values are around the limit value for slender sections of 45, and the roof rails are

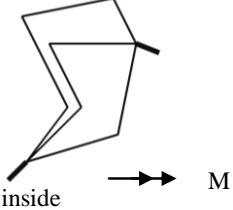
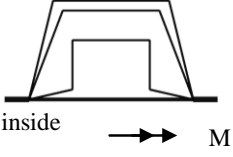
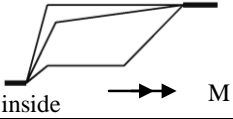
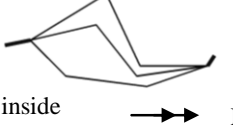
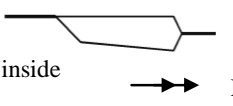
	Pillar profile	I (mm ⁴) Z (mm ³) S (mm ³)	I_{perf} (mm ⁴) Z_{perf} (mm ³) S_{perf} (mm ³)	Slenderness +bending λ_s
A pillar		389000 7482 9128	344000 6896 8413	40.2
B pillar		217500 6721 7460	190300 6368 7068	45.7
C pillar		114300 3967 4443	106800 3582 4012	48.0
D pillar		143700 3400 3944	130300 3176 3684	42.4
Roof rails		12830 951 1065	9428 639 716	64.7

Fig. 5 Profiles of the exemplar vehicle. I = second moment of area, Z = elastic bending modulus, S = plastic bending modulus, $perf$ = 50% perforation of the inside element, *inside* indicates the inside of the vehicle, M = bending moment positive axis

very slender. It is also clear that the bending properties of the roof rails are significantly smaller than those for the pillars (around 10 times or more).

Perforations were introduced in the analysis since typical roof structure profiles frequently include perforations of up to 60% of the element width, and the plastic hinges might form at these locations. A nominal perforation of 50% of the element width was introduced into the profiles on the element corresponding to the inside of the vehicle. The geometric properties were calculated for the perforated sections and are listed in Fig. 5.

5.2 Collapse load and energy dissipated in different rollover mechanisms

All ten mechanisms in Fig. 1 were analysed for the exemplar vehicle. For each mechanism in

Table 1 Results of the parametric study of varying the geometric and material properties of the profiles of the exemplar vehicle. F = collapse load, E = collapse energy dissipated. *Original* is the actual vehicle profile geometry. *Modified* is for: increasing the steel sheet thickness 2 times ($2t$); increasing the material yield stress 2 times ($2f_y$); and increasing both the thickness and yield stress 2 times ($2t, 2f_y$). *Perforated (perf)* is a perforation of 50% of the inside element width of the profile.

Mechanism (Fig. 1)	Original		Original perforated		Modified E/E_0			Modified F/F_0		
	Energy E_0 (J)	Collapse load F_0 (kN)	E_{perf}/E_0	F_{perf}/F_0	$2f_y$	$2t$	$2f_y, 2t$	$2f_y$	$2t$	$2f_y, 2t$
1	1262	11.8	0.92	0.91	1.27	3.31	5.34	1.42	2.99	5.27
2	1632	8.5	0.93	0.94	1.38	2.93	4.66	1.43	2.78	5.05
3	2197	6.9	0.94	0.97	1.50	2.91	4.40	1.43	2.60	4.87
4	1426	7.6	0.94	0.95	1.40	3.04	5.03	1.43	2.69	4.96
5	2049	6.5	0.95	0.98	1.53	2.99	4.61	1.43	2.55	4.81
6	2231	13.4	0.94	0.97	1.38	3.24	5.78	1.43	2.58	4.84
7	2474	10.0	0.96	1.00	1.44	3.01	4.41	1.43	2.44	4.72
8	4205	18.6	0.96	1.01	1.51	3.03	4.75	1.43	2.37	4.65
9	2308	14.8	0.94	0.98	1.40	3.24	5.74	1.43	2.53	4.79
10	4952	26.1	0.96	1.01	1.57	3.00	4.68	1.43	2.36	4.64
		Mean:	0.95	0.97	1.44	3.07	4.94	1.43	2.59	4.86

Fig. 1 the magnitude of hinge rotation at each hinge in each pillar was determined, and the collapse load and energy dissipated were calculated, and the results are tabulated in Table 1. For the collapse load only the front (A-pillar) frame was analysed, and for the energy dissipated all three roof frames were assumed to deform equally. Significant differences in the amount of energy dissipated may be calculated for the various mechanisms, depending on the relative amount of deformation in the pillars and roof rails, since the pillars are much stronger than the roof rails (Table 1). For example, mechanism 10 dissipates nearly 4 times as much energy as mechanism 1, since mechanism 1 involves extensive deformation of the roof rails whereas mechanism 10 involves extensive deformation of the stronger pillars. Mechanism 10 also undergoes much more severe overall deformation than mechanism 1. An example calculation is shown in Appendix A.

Since the perforation position was not known a priori, the mechanisms were analysed with all or none of the profiles perforated. The experimental results on hat sections indicated that for compact sections there is a large effect of perforations on the energy dissipation capability due to the large reduction in section ductility, while conversely for slender sections the perforations have negligible effect on the energy dissipation since slender sections already have little ductility. This behaviour was discussed more extensively in Bambach *et al.* (2009). In the original roof structure of the exemplar vehicle the components were all relatively slender, and in accordance with the experimental results the effect of perforations was small with mean reductions in collapse load and energy dissipation of only 3% and 5%, respectively, in Table 1.

6. Optimisation study of the geometric and material properties of the roof structure components

In order to demonstrate the application of the method to optimise the roof structure components

for increased roof collapse resistance, parametric studies of the geometric and material properties of the pillars and roof rails were performed and their effect on the collapse load and energy dissipation of the vehicle roof frame were determined. All ten mechanisms in Fig. 1 were analysed. The effects of: increasing the steel sheet thickness 2 times ($2t$); increasing the material yield stress 2 times ($2f_y$); and increasing both the thickness and yield stress 2 times ($2t, 2f_y$), were analysed, and the results are tabulated in Table 1.

When the steel thickness is doubled, the moment capacity is increased since the capacity is directly proportional to the geometric properties of the section. However, doubling the material thickness also halves the section slenderness, thus the moment capacity is non-linearly related to the thickness. In the present case study the original profiles of the exemplar vehicle are relatively slender, and doubling the thickness produces compact sections which more than doubles the moment capacity and collapse load. Additionally, as the slenderness is reduced the ductility is increased, thus the energy dissipation is also non-linearly related to the thickness. Doubling the thickness produces compact sections which may develop significant in-plane plasticity, which results in an average increase in collapse load and energy dissipation of 2.59 and 3.07 times, respectively, in Table 1.

When the steel yield stress is doubled, the moment capacity is increased since the capacity is directly proportional to the yield stress. However, doubling the yield stress also increases the section slenderness by 1.41 times, thus the moment capacity is non-linearly related to the material yield stress. In the present case study the original profiles of the exemplar vehicle are relatively slender, and doubling the yield stress produces even more slender sections which less than doubles the moment capacity and collapse load. Additionally, as the slenderness is increased the ductility is reduced, thus the energy dissipation is also non-linearly related to the yield stress. Doubling the yield stress of all profiles results in an average increase in collapse load and energy dissipation of 1.43 and 1.44 times, respectively, in Table 1. If the yield stress and the material thickness are both doubled, mean increases in collapse load and energy dissipation of 4.86 and 4.94 times, respectively, are achieved in Table 1.

7. Limitations

It should be noted that in real-world rollover crashes the roof structure is not the only component which dissipates energy (e.g., the roof and side panels, interior elements and glass elements). In many real-world rollover crashes other crash types may also occur or even trigger the rollover, such as side/rear/frontal impacts with other vehicles or foreign objects. Many of these mechanisms are clearly dependant on the characteristics of the particular rollover event being studied.

In the present paper all of the analytical formulae have been developed for static bending, while a vehicle rollover will of course be a dynamic event. Recent experimental and analytical studies on steel square hollow sections subjected to transverse impacts that result in large plastic bending deformation have been presented (Bambach *et al.* 2008, Bambach 2011). It was shown that the dynamic plastic mechanism forms in the same manner as the static one, and that the application of the load dynamically only slightly increases the capacity and energy dissipation. This is due to the strain-rate sensitivity of the yield stress of steel, however as the strain is increased beyond the yield strain the sensitivity of steel reduces. It was thus concluded that strain-rate effects do not play an important role in structures undergoing large plastic bending deformation at relatively low

strain rates, and this has also been shown by a number of other authors as discussed in Bambach *et al.* (2008), Bambach (2011). Thus only small increases in the collapse load and energy dissipated calculated with the quasi-static approach presented in this paper could be expected for real-world rollovers, while the comparisons between the geometric and material properties would be unchanged (since the strain-rate effect will be the same in all cases).

It should be noted that the mechanisms presented in Fig. 1 are idealisations of observed mechanisms, and in some cases may not be attainable exactly. However, the angle magnitudes may be adjusted by the analyst to better represent particular, observed mechanisms. The influence of perforations on the collapse load and energy absorption was investigated, however these were based upon idealised perforations introduced in the experiments in Bambach *et al.* (2009), rather than exact observed geometry and perforation localisations in vehicles. These factors (not only percentage of cross-section area) may influence the ultimate load and crushing behaviour, however were not analysed in the present study. The analytical method developed in this study is an approximate one, and experimental verification (using finite element simulations) for selected case(s) is recommended, and is a topic for future study.

8. Conclusions

An analytical technique has been presented by which the collapse load and energy dissipating capacity of the roof structure of a vehicle subjected to a rollover collapse may be determined. The procedure covers many collapse mechanisms typically observed in real-world vehicle rollover crashes, is applicable to most typical vehicle profile geometries, and is presented in a generic fashion such that it may be applied by an analyst to any vehicle. A case study was presented for a late model exemplar vehicle, in which the procedure is developed and a number of optimisation studies related to the geometric and material properties of the roof structure components have been demonstrated. The procedure will improve forensic crash reconstruction of vehicle rollover crashes by enabling the analyst to estimate the kinetic energy that was dissipated by the roof structure during the rollover event. It may also be useful for analytical studies of roof strength and energy dissipation potential of vehicle roof structures in order to optimise roof designs and reduce occupant injury potential in vehicle rollover crashes.

References

- AS 4100 (1998), *Australian Standard, Steel Structures*, Standards Australia, Sydney.
- Bambach, M.R., Jama, H.H., Zhao, X.L. and Grzebieta, R.H. (2008), "Hollow and concrete filled steel hollow sections under transverse impact loads", *Eng. Struct.*, **30**(10), 2859-2870.
- Bambach, M.R., Tan, G. and Grzebieta, R.H. (2009), "Steel spot-welded hat sections with perforations subjected to large deformation pure bending", *Thin Wall. Struct.*, **47**(11), 1305-1315.
- Bambach, M.R. (2011), "Design of hollow and concrete filled steel and stainless steel tubular columns for transverse impact loads", *Thin Wall. Struct.*, **49**(10), 1251-1260.
- Bambach, M.R., Grzebieta, R., McIntosh, A.S. and Mattos, G. (2013), "Cervical and thoracic spine injury from interactions with vehicle roofs in pure rollover crashes", *Accid. Anal. Prevent.*, **50**, 34-43.
- Elchalakani, M. and Fernando, D. (2012), "Plastic mechanism analysis of unstiffened steel I-section beams strengthened with CFRP under 3-point bending", *Thin Wall. Struct.*, **53**, 58-71.
- Elchalakani, M. (2007), "Plastic mechanism analyses of circular tubular members under cyclic loading",

- Thin Wall. Struct.*, **45**(12), 1044-1057.
- Elchalakani, M., Zhao, X.L. and Grzebieta, R.H. (2002), "Plastic mechanism analysis of circular tubes under pure bending", *Int. J. Mech. Sci.*, **44**(6), 1117-1143.
- Kecman, D. (1983), "Bending collapse of rectangular and square section tubes", *Int. J. Mech. Sci.*, **25**(9-10), 623-36.
- Kotelko, M. (2008), "Alternative solutions of the problem of load-capacity of thin-walled plated structures", *Mech. Mech. Eng.*, **12**(4), 323-336.
- Maduliat, S., Bambach, M.R. and Zhao, X.L. (2012), "Yield line mechanism analysis of cold-formed channel sections with edge stiffeners under bending", *Struct. Eng. Mech.*, **42**(6), 883-897.
- NHTSA (2013), *Traffic Safety Facts: Passenger Vehicles: 2011 Data*, DOT HS 811 827.
- NHTSA (2012), National Automotive Sampling System (NASS), Crashworthiness Data System (CDS), Accessible at: <http://www.nhtsa.gov/NASS>.
- Papangelis, J.P. and Hancock, G.J. (1995), "Computer analysis of Thin-Walled Structural Members", *Comput. Struct.*, **56**(1), 157-176.
- Setiyono, H. (2007), "Plastic mechanism and elastic-analytical approaches applied to estimate the strength of an axially compressed-thin-walled channel steel section beam", *Int. J. Mech. Sci.*, **49**(3), 257-266.
- Sharma, D., Stern, S., Brophy, J. and Choi, E. (2007), "An overview of NHTSA's crash reconstruction software", *20th Enhanced Safety of Vehicles Conference Proceedings*, Paper 07-0211, Lyon, France.
- Tan, G., Bambach, M.R. and Grzebieta, R.H. (2008), "Database of Australian vehicle pillar profiles - General profiles and profiles from vehicles involved in rollover crashes", Monash University, Research Report No RR8.
- Ungureanu, V., Kotelko, M., Mania, R.J. and Dubina, D. (2010), "Plastic mechanisms database for thin-walled cold-formed steel members in compression and bending", *Thin Wall. Struct.*, **48**(10-11), 818-826
- Ye, J.H., Zhao, X.L., Van, B.D. and A-Mahaidi, R. (2007), "Plastic mechanism analysis of fabricated square and triangular sections under axial compression", *Thin Wall. Struct.*, **45**(2), 135-148.
- Young, D., Grzebieta, R.H., Bambach, M.R., McIntosh, A. and Frechede, B. (2007), "Diving vs Roof Intrusion: a review of rollover injury causation", *Int. J. Crashworth.*, **12**(6), 609-628.

Appendix A

Fig. A1 presents an example calculation of the energy dissipated by the exemplar vehicle subjected to rollover mechanism 1 (Fig. 1). The full calculation for the A-pillar is shown. The calculations for the other pillars and roof rails are not shown, but follow that for the A-pillar.

$$E := 200000 \cdot \text{MPa} \quad f_y := 250 \cdot \text{MPa} \quad t := 0.9 \cdot \text{mm} \quad \lambda_y := 45 \quad \lambda_p := 30 \quad m_p := 0.25 \cdot f_y \cdot t^2$$

Energy absorbed by the A pillar under total deformation +0.26 radians

$$I := 389000 \cdot \text{mm}^4 \quad Z := 7482 \cdot \text{mm}^3 \quad S_{xx} := 9128 \cdot \text{mm}^3 \quad cf_{\text{pos}} := 38 \cdot \text{mm} \quad \lambda := \frac{cf_{\text{pos}} - 2 \cdot t}{t} \cdot \sqrt{\frac{f_y}{250 \cdot \text{MPa}}}$$

$$\lambda = 40.2 \quad M_A := \text{if} \left[\lambda \leq \lambda_p, S \cdot f_y, \text{if} \left[\lambda > \lambda_y, \frac{\lambda_y}{\lambda} \cdot f_y \cdot Z, \left[\left[\frac{\lambda_y - \lambda}{\lambda_y - \lambda_p} \cdot (S - Z) \right] + Z \right] \cdot f_y \right] \right] \quad M_A = 2 \text{ kN} \cdot \text{m}$$

$$R_A := \text{if} \left[\lambda \leq \lambda_p, \frac{\lambda_p}{\lambda} \cdot 5, \text{if} \left[\lambda > \lambda_y, 1, \left[\left(\frac{\lambda_y - \lambda}{\lambda_y - \lambda_p} \cdot 4 \right) + 1 \right] \right] \right] \quad R_A = 2.274$$

$$\theta_{\text{max}} := \left(\frac{35 \cdot m_p \cdot 80 \cdot \text{mm}}{M_A} \right)^2 \quad \theta_y := \frac{Z \cdot f_y \cdot 700 \cdot \text{mm}}{E \cdot I}$$

$$W_A := 0.5 \cdot M_A \cdot \theta_y + (R_A - 1) \cdot M_A \cdot \theta_y + 70 \cdot m_p \cdot 80 \cdot \text{mm} \cdot \left(\sqrt{0.26 + \theta_{\text{max}} - R_A \cdot \theta_y} - \sqrt{\theta_{\text{max}}} \right) \quad W_A = 175 \text{ J}$$

Energy absorbed by the B, C and D pillars under total deformation +0.26 radians

$$W_B := 136 \cdot \text{J} \quad W_C := 113 \cdot \text{J} \quad W_D := 127 \cdot \text{J}$$

Energy absorbed by the roof rails under total deformation +0.26, -1.13, +1.57, and -0.96 radians

$$W_{R_{\text{pos}0.26}} := 25 \cdot \text{J} \quad W_{R_{\text{neg}1.13}} := 65 \cdot \text{J} \quad W_{R_{\text{pos}1.57}} := 89 \cdot \text{J} \quad W_{R_{\text{neg}0.96}} := 58 \cdot \text{J}$$

The entire roof structure is assumed to collapse in the mechanism, that is all three frames of the roof structure. The frames are thus; 1. A pillars and roof rail, 2. B pillars and roof rail, 3. C and D pillars and roof rail. The total energy absorbed by mechanism 1 with a post-crash angle of 0.26 radians (Figure 1) is:

$$W_{\text{total}} := W_A + W_B + W_C + W_D + 3 \cdot (W_{R_{\text{pos}0.26}} + W_{R_{\text{neg}1.13}} + W_{R_{\text{pos}1.57}} + W_{R_{\text{neg}0.96}})$$

$$W_{\text{total}} = 1262 \text{ J}$$

Fig. A1 Example calculation of the energy dissipated by the exemplar vehicle subjected to rollover mechanism 1 (Fig. 1)